Composite Structures 101 (2013) 104–110

Contents lists available at SciVerse ScienceDirect

Composite Structures

journal homepage: www.elsevier.com/locate/compstruct

Simultaneously high stiffness and damping in a class of wavy layered composites

Trisha Sain [a], Julien Meaud [b], Greg Hulbert [b], Ellen M. Arruda [c], Anthony M. Waas [a,*]

[a] Department of Aerospace Engineering, Composite Structures Laboratory, University of Michigan, Ann Arbor, MI 48109, United States
[b] Department of Mechanical Engineering, University of Michigan, Ann Arbor, MI 48109, United States
[c] Department of Mechanical Engineering, Biomedical Engineering and Program in Macromolecular Science and Engineering, University of Michigan, Ann Arbor, MI 48109, United States

ARTICLE INFO

Article history:
Available online 16 February 2013

Keywords:
Damping
Stiffness
Wavy layer
Polymer
Composite

ABSTRACT

We present results for stiffness and damping prediction in a class of layered, wavy, metal–polymer composites that exceed conventionally published stiffness-damping maps (The Wang–Lakes line, see [14]). These composites are realized by judiciously placing selected, wavy, metal sheets that sandwich an ultra-thin layer of polymer. Stacks of alternating metal–polymer layered composites, when compressed axially under harmonic loading exhibit not only very high stiffness but also very high damping leading to an "ideal" combination of properties for a variety of structural applications. In this paper, a finite element based study has been presented to predict the mechanical stiffness and damping of such composites. It has been shown that reducing the thickness of the viscous polymer layer not only increases the stiffness of such composites but also improves the damping.

1. Introduction

The use of tailored composites for improved stiffness/strength and enhanced damping performance is becoming increasingly important in advanced engineering systems that are considered for aerospace and automotive applications. Stiffness improvement in composites can be achieved by controlling the manufacturing and constituent properties starting from the nano scale and spanning up to the traditional macro-composite manufacturing methods. In particular, polymer composites have generated significant interest in the design of damped structural systems, due to the viscoelastic properties of the polymer. From previous research, it appears that design changes that cause an increase in damping will result in corresponding reduction in stiffness and strength [1]. At the macro-mechanical level, research has emphasized that individual constituent layer properties, orientation, interlaminar effects, hybridization of laminae, etc. may have a significant influence on the attainment of improved damping properties. The results presented by Hwang and Gibson [3] for graphite/epoxy angle ply laminated composites under extensional vibrations, showed the existence of an optimal fiber orientation and an optimal laminate width to thickness ratio for maximizing the contribution of interlaminar damping. The data showed the maximum loss factor that could be achieved for this composite is in the range of 0.02–0.025 for a fiber orientation of 40°. The use of surface damping treatments by the application of a viscoelastic damping tape sandwiched between the base structure and a thin constraining layer is also well known. In this type of structure, damping is improved due to the fact that vibration energy will be dissipated by shearing motion of the viscoelastic material, as the base structure vibrates in flexure [2]. It has also been shown in [5], that damping due to constrained layer treatment can be optimized by selecting the proper length of the constraining layers. Analytical and experimental results have been presented in [5] to show that an optimum tape-to-beam length ratio leads to maximum damping, and exceeding that length does not necessarily improve the damping characteristic. At the same time it is observed that for a given tape-to-beam length ratio damping is higher when the tape is fixed at the root than the case where it is free. This effect was shown to be due to additional shear deformation created in the visco-elastic layer by the fixed boundary condition.

In the micro-mechanics based approach of damping improvement, the effects of fiber aspect ratio and fiber orientation have been explored. Suarez et al. [6] and Gibson et al. [7] showed that the use of discontinuous fiber reinforcement with a stiffness mismatch between fiber and matrix leads to the improvement of internal damping in fiber reinforced polymer composite materials by increasing the shear deformation near the fiber ends. It was also shown that for unidirectional short fiber composites damping increases with decreasing fiber aspect ratio. More in this line, the effect of fiber interaction on damping improvement is studied experimentally and analytically, by varying the fiber end gap (i.e. the distance between two successive fiber) [3]. The conclusion was that the composite damping generally increases with increasing fiber end gap size, because of the stress transfer through a shear mechanism at the fiber matrix interface and an increased amount of matrix material between two fiber ends. However, for

* Corresponding author. Tel.: +1 734 764 8227.
E-mail address: dcw@umich.edu (A.M. Waas).

0263-8223/$ - see front matter © 2013 Elsevier Ltd. All rights reserved.
http://dx.doi.org/10.1016/j.compstruct.2013.01.024

all these cases, the stiffness of the composite reduces due to the discontinuous fiber alignment. In other words, all these micro-mechanical approaches of improving damping can be achieved at the cost of reducing the composite stiffness.

In the micro-scale and nano scale based studies, effects of the fiber matrix interphase and its influence on damping has been investigated. Various 2D and 3D finite element models are found to characterize the interphase contribution on damping such as in, [8,9]. Friend et al. [9] assumed a two phase composite material as perfectly bonded and interphase as a three-phase material and concluded that interphase has a significant influence on composite damping. The important point to note here is that influence of interphase is most likely to happen in micro level or even smaller length scale, its effect is not so significant at the macroscopic structural property evaluation.

Another important approach with relevance to the present study, by Pratt et al. [10,11] has been devoted to investigating the geometric fiber wavy pattern in composites to induce additional damping. This particular manufacturing technique involved the use of visco-elastic layers that are co-cured with and embedded between fiber layers having continuous wave-like patterns. In another study, Pratt [12], showed a detailed FEA analysis and comparison with experimental results of this type of wavy layer composite in order to show the variation of its stiffness or damping characteristics as a function of the thickness of the composite layer, thickness of the visco-elastic layer and the variation in the wavelength. Their results show, for a given composite layer thickness, by reducing the thickness of the visco-elastic layer, the damping property can be improved, while keeping the modulus more or less constant. Meaud et al. [4] recently derived analytical formulae for the effective stiffness and damping of linear viscoelastic composites with parallel plane layers of a soft and lossy constituent and a stiff constituent. They demonstrated using numerical optimization that high damping and high stiffness can be simultaneously obtained. In the present work, a numerical study is performed by exploiting the concept of sandwiching an ultra thin polymer layer in between thick *wavy* steel layers, to improve the 'in-plane' stiffness and damping properties of the resulting composite. It is observed that for a given amplitude of the waviness, by reducing the thickness of the visco-elastic polymer layer, *both* stiffness and damping can be improved by a significant amount. The explanation for this improvement is due to the relative increase in the steel volume fraction; reducing the polymer layer thickness, for a given composite thickness, increases the volume fraction of the steel, which contributes to improved in-plane stiffness. Moreover, shear dissipation mechanism as described earlier is involved in the polymer layer which results in improved damping properties. The accurate modeling of the visco-elastic polyurethane is a key to the present predictive numerical study, which has been achieved through a micro-mechanical based constitutive model in conjunction with appropriate experimental data fitting. The numerical results show promising values for the composite stiffness and damping, well above the Wang and Lakes line [14].

2. Problem description and numerical implementation

We restrict the geometric parameters considered herein to those that are feasible using current manufacturing technologies [20]. The manufacturing facility suggests that the minimum possible thickness of the polymer layer can be 2 μ, and it can be varied up to a maximum limiting value of 20 μ. For the finite element (FE) simulations, these two values are taken to be the limiting cases for the polymer layer thickness. A series of simulations is performed by varying many of the geometric features, such as the amplitude of the waviness (δ), thickness of the metal sheets (t_s), and thickness of the polymer layer (t_p), to achieve the maximum possible stiffness and damping with this configuration. A 2D plane strain representative volume element (RVE) is chosen for the simulation, as shown in Fig. 1, where the plane strain condition is restricted to the x–y plane. Periodic boundary conditions are applied along the edges of the RVE. The waviness of the metal sheet is sinusoidal in nature, to avoid sharp joints (corners at the peak) in manufacturing and provide a more stable structure. The material models used in the simulations are perfectly elastic for the metal sheet with no damping, and a nonlinear viscous material model for the polymer layer. The nonlinear viscous model used here has been proposed by Sain et al. [18], as a modification of a simple linear-viscous law to capture the strain rate dependent damping response of the chosen polymer in the small strain regime. The particular polymer chosen here is a polyurethane synthesized in-house by our collaborators (hereby named as UMPU2), which shows considerably large damping using dynamic mechanical analysis (DMA) characterization with $tan\delta = 0.98$ and a storage modulus of 60 MPa at 1 Hz frequency. To capture this high amount of damping along with the strain rate dependent nature of this class of polymers, a nonlinear visco-elastic constitutive model is proposed in [18]. Since the entire modeling methodology is described in detail in [18], only a summary has been provided in the following.

2.1. Constitutive modeling of polyurethane: rate dependent damping and stiffness characterization

1-D schematic representation of the constitutive model is shown in Fig. 2. The model consists of several branches of linear spring and dashpot combinations, which takes into account the entire range of the relaxation spectrum. The modification in the present model compared to a traditional linear visco-elastic model essentially lies in adding the hyper-elastic spring to capture the high stretch behavior in the polymer along with the linear spring dashpot behavior within a finite deformation framework. To obtain the linear spring and dashpot constants, the constitutive equations

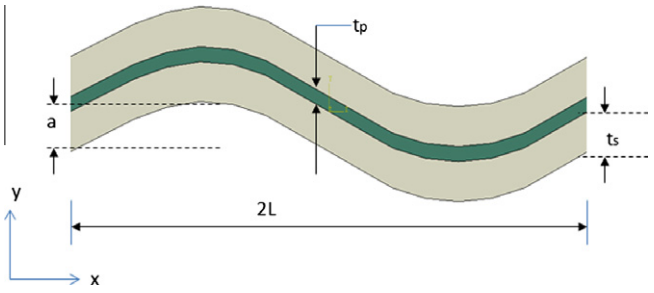

Fig. 1. The representative volume element of the proposed composite.

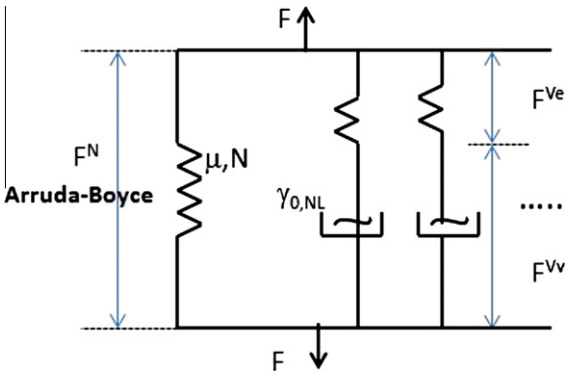

Fig. 2. Schematic representation of the constitutive model for the polyurethane.

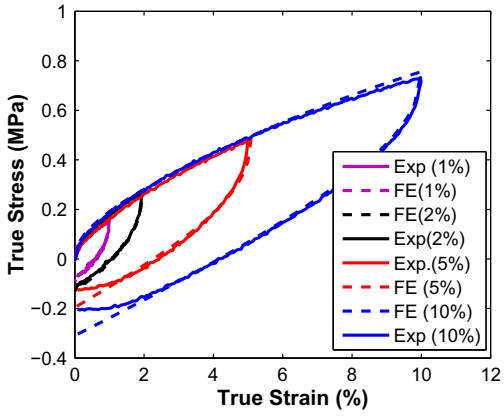

Fig. 3. Uniaxial stress–strain response for UMPU at quasi-static strain rate (0.5%/s)-comparison of experimental data and FE model prediction.

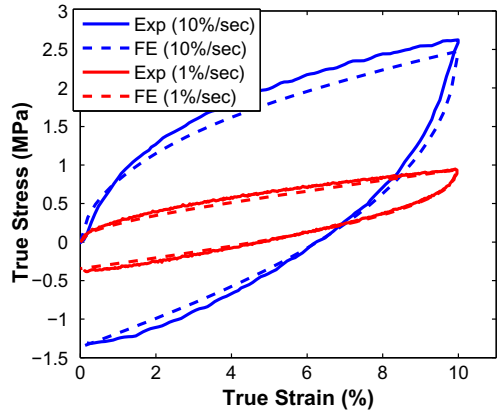

Fig. 4. Uniaxial stress–strain response at high strain rate-comparison of FE model prediction and experimental data.

are linearized and represented by an equivalent Prony series based model and experimental DMA data is used to fit the relaxation time constants. Each term in the Prony series expression represents a stiffness value corresponding to a particular relaxation time. Hence, the total number of terms in Prony series needed to fit the DMA data for the UMPU2 depends on how many relaxation times are present to characterize the material response for the frequency/strain rates considered. For the UMPU2 polyurethane used in this study, it is observed that 5 branches of linear spring-dashpot combination (or five terms in Prony series) is required to capture the frequency dependent stiffness and damping variation of the DMA data. As shown in Fig. 2, the left most side branch consists of a nonlinear spring and there are several branches of linear springs in combination with linear dashpot. The macroscopic deformation gradient $\mathbf{F}$ is the same in all the branches as given by:

$$\mathbf{F} = \mathbf{F}^N = \mathbf{F}^{V1} = \mathbf{F}^{V2} = \cdots \tag{1}$$

and the total Cauchy stress is the sum of the components coming from all the springs (in this case $n = 5$),

$$\mathbf{T} = \mathbf{T}^N + \sum_{i=1}^{n} \mathbf{T}^{Vi} \tag{2}$$

The hyperelastic rubbery spring captures the high stretch deformation in the molecular chains. The well known Arruda–Boyce [17,19] eight chain model is used to characterize the nonlinear spring deformation. The Cauchy stress in the non linear spring following Arruda–Boyce potential is given as:

$$\mathbf{T}^N = \frac{nk\theta}{3J}\frac{\sqrt{N}}{\lambda_{chain}} L^{-1}\left(\frac{\lambda_{chain}}{\sqrt{N}}\right)\overline{\mathbf{B}}' \tag{3}$$

with n being the chain density (number of molecular chains per unit reference volume) of the underlying macromolecluar network, k is the Boltzmann's constant and θ is the absolute temperature, currently taken as constant room temperature. Further N is the number of rigid links between two crosslinks and $\sqrt{N}$ represents the limiting stretch of each chain.

In Eq. (3), $\overline{\mathbf{B}}$ is the right Cauchy Green strain given by,

$$\overline{\mathbf{B}} = \overline{\mathbf{F}}^N \overline{\mathbf{F}}^{N^T} \tag{4}$$

and $\overline{\mathbf{B}}'$ is the deviatoric component of $\overline{\mathbf{B}}$ as given by,

$$\overline{\mathbf{B}}' = \overline{\mathbf{B}} - tr(\overline{\mathbf{B}}/\mathbf{3}) \tag{5}$$

The isochoric deformation is developed by neglecting the volume change as:

$$\overline{\mathbf{F}}^N = J^{-1/3}\mathbf{F}^N \tag{6}$$

In Eq. (3), L^{-1} is the inverse Langevin function, given by

$$L^{-1}(\xi) = \xi\frac{3-\xi^2}{1-\xi^2} \tag{7}$$

In Eq. (3), λ_{chain} is the stretch on each chain in the network as given by $\lambda_{chain} = \sqrt{I_1/3}$, with $I_1 = tr(\overline{\mathbf{B}})$ as the first invariant of $\mathbf{B}$.

2.2. Kinematics of the Maxwell element

To describe the kinematics of the five linear spring-dashpot branches, it is expedient to explain the kinematics just for one branch considering the traditional Maxwell element in finite deformation regime. We assume that the total deformation gradient can be multiplicatively decomposed into an elastic part $\mathbf{F}^{V^e}$ and a viscous part $\mathbf{F}^{V^v}$ as [15,16]:

$$\mathbf{F}^V = \mathbf{F}^{V^e}\mathbf{F}^{V^v} \tag{8}$$

Furthermore, we introduce the relation between the velocity gradient, rate of total deformation tensors and the rate of viscous strain tensor (in the current configuration) as follows,

$$l^V = \dot{\mathbf{F}}^V\mathbf{F}^{V-1} = \dot{\mathbf{F}}^{V^e}\mathbf{F}^{V^{e-1}} + \mathbf{F}^{V^e}.(\dot{\mathbf{F}}^{V^v}\mathbf{F}^{V^{v-1}})\mathbf{F}^{V^{e-1}} \tag{9}$$

Hence, in the reference configuration, the visco-plastic velocity gradient can be written as:

$$\mathbf{L}^{V^v} = \mathbf{D}^{V^v} + \mathbf{W}^{V^v} = \dot{\mathbf{F}}^{V^v}\mathbf{F}^{V^{v-1}} \tag{10}$$

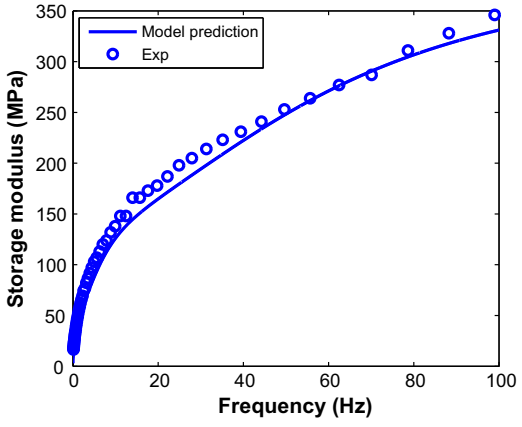

Fig. 5. Comparison of the model prediction and the experimental data- storage modulus.

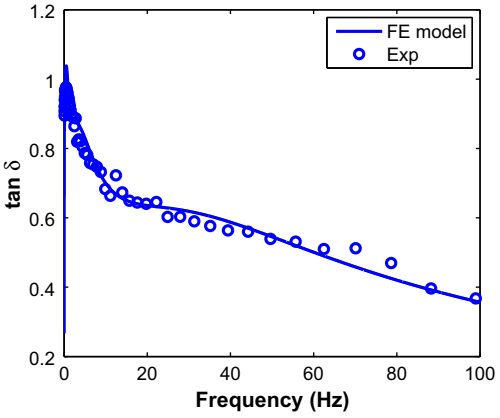

Fig. 6. Comparison of the model prediction and the experimental data-tan δ.

where $\mathbf{D}^{Vv}$ is the rate of viscous strain and $\mathbf{W}^{Vv}$ is the viscous spin tensor respectively. Without loss of generality, one can assume the viscous spin to be zero and the viscous flow rule is expressed as:

$$\mathbf{D}^{Vv} = \frac{\dot{\gamma}_d^{Vv}}{\sqrt{2}\bar{\tau}_v}\mathbf{T}^{v\prime} + \frac{\dot{\gamma}_P^{Vv}}{\sqrt{2}\bar{\tau}_v}P\mathbf{I} \tag{11}$$

where P is the hydrostatic pressure. In most models, the viscous stretch rate is assumed to depend only on the deviatoric component of the driving Cauchy stress (the first term in the right hand side of Eq. (11)). However we found necessary to include a small component that depends on the hydrostratic pressure in the viscous stretch rate in order to fit the DMA data (the 2nd term in the right hand side of Eq. (11)). The equivalent stress $\bar{\tau}_v$ is given by

$$\bar{\tau}_v = \left[\frac{1}{2}\mathbf{T}^{v\prime} : \mathbf{T}^{v\prime}\right]^{1/2} \tag{12}$$

where $\mathbf{T}^{v\prime}$ is the deviatoric component of the Cauchy stress developed in the linear spring attached with the dashpot. The constitutive equation to describe the stress–strain response in the linear spring is given by,

$$\mathbf{T}^{V} = \frac{1}{(det\mathbf{F}^{Ve})}\mathbf{L}^{e}(ln\mathbf{V}^{Ve}) \tag{13}$$

where $\mathbf{V}^{Ve}$ is the right stretch tensor obtained by polar decomposition of the elastic deformation gradient as,

$$\mathbf{F}^{Ve} = \mathbf{V}^{Ve}\mathbf{R}^{Ve} \tag{14}$$

and $\mathbf{L}^{e}$ is the fourth order elastic tensor.

In Eq. (11), $\gamma_d^{\dot{V}v}$ and $\gamma_P^{\dot{V}v}$ are the equivalent viscous strain rates due to the deviatoric stress and due to the hydrostatic pressure respectively, and are assumed to follow a linear viscous law. Moreover, the viscous laws for deviatoric and volumetric deformations are assumed to have the same relaxation time constant, t_r. For a linear viscoelastic model, the relationship between the strain rate and the stress in linear small strain regime is given by:

$$\dot{\epsilon} = \frac{dev(\sigma)}{2Gt_r} + \frac{tr(\sigma)}{3Kt_r} \tag{15}$$

In order for the finite deformation model to be equivalent to a linear viscoelastic model described by Eq. (15) in the low strain regime, the equivalent viscous strain rates are given by:

$$\gamma^{\dot{V}v} = \frac{\sqrt{2}\bar{\tau}_v}{2Gt_r} \tag{16}$$

$$\gamma^{\dot{V}v} = \frac{\sqrt{2}\bar{\tau}_v}{3Kt_r} \tag{17}$$

where G (respectively K) is the shear modulus (respectively bulk modulus) corresponding to the elastic spring. This equivalence is important so that the time constants and spring constants found from the frequency domain Prony series fit into the proposed finite deformation visco-elastic model. The proposed model is implemented in ABAQUS Explicit software by writing a user material subroutine VUMAT and a rigorous validation was done using various experimental data. The validation of the proposed constitutive model is necessary for a wide range of strain rates, as the polymer inside the composite structures is subjected to different strain rates due to heterogeneous strain distribution. Hence the accuracy of the prediction for the damping and stiffness of the wavy composites will depend on how good the polymer material model can capture the UMPU2 response as a function of strain rate. The material parameters as reported in Table 1, are subsequently used in finite deformation constitutive update written in the form of VUMAT, to predict the experimental response. Fig. 3, shows the comparison between the finite element prediction and experimental results on PU sample, loaded quasi-statically (0.5%/s) at different strain levels and unloaded subsequently. The model prediction has an excellent agreement in terms of capturing both the loading and unloading response until 10% strain. Simulations also performed to predict the high rate loading–unloading response. Fig. 4 shows the FE prediction and experimental data for loading and unloading at two different rates 1%/s and 10%/s respectively. It is seen that FE predictions have excellent match with experiments for a wide range of strain rate 0.5–10%/s to capture the uniaxial response. Further simulations were performed to predict the storage modulus and damping *tan*δ at different frequency. A sinusoidal strain pulse with an amplitude of 0.1% is given as an input for a frequency range of 0.1–100 Hz to simulate the DMA measurements. The storage modulus is measured from the ratio between stress output and the maximum strain input whereas the phase lag between the input (strain) and output (stress) response is used to calculate *tan*δ. The comparison between FE predicted DMA values and experimental data are shown in Fig. 5 and Fig. 6, which once again has a good agreement over the entire frequency range.

Table 1
Material parameters for polyurethane.

i	1	2	3	4	5
G_i (MPa)	4.04	15.04	1.85	107.45	43.28
t_{ri} (s)	1.121	0.163	22.951	0.0023	0.023

2.3. Characterizing damping in the nonlinear regime

Since the polymeric material response can be nonlinear locally even when the global input strain is low in a heterogeneous

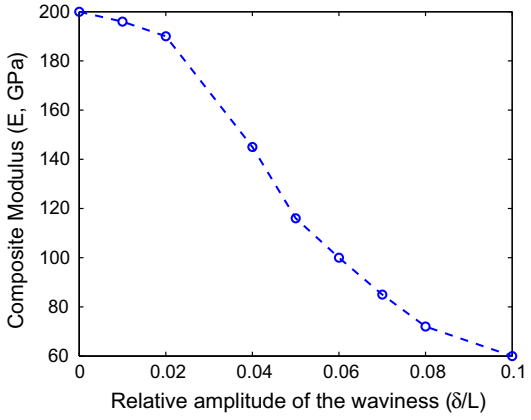

Fig. 7. Composite stiffness (axial) as a function of relative amplitude of the waviness for $t_p = 0.002$ mm and $t_s = 0.05$ mm.

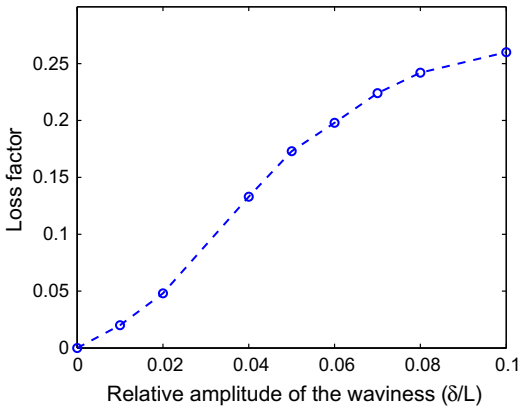

Fig. 8. Loss factor as a function of relative amplitude of the waviness for $t_p = 0.002$ mm and $t_s = 0.05$ mm.

composite material, it is important to introduce the definition of material damping in the nonlinear viscoelastic regime. When the material behavior is linear visco-elastic, the well known concept of phase lag can be used to characterize the material damping. For such materials, given a sinusoidal force/stress input of amplitude σ_0 and frequency ω the response will be a sinusoidal displacement/strain of amplitude ϵ_0 with a phase lag δ in time t as follows:

$$\epsilon = \epsilon_0 \sin(t\omega) \tag{18}$$

and

$$\sigma = \sigma_0 \sin(t\omega + \delta) \tag{19}$$

Then, the loss modulus and storage modulus are defined as

$$E'' = \frac{\sigma_0}{\epsilon_0} \sin\delta \tag{20}$$

and

$$E' = \frac{\sigma_0}{\epsilon_0} \cos\delta \tag{21}$$

respectively. The damping in the material is thereby characterized through $\tan\delta$ as the ratio between loss modulus and storage modulus as:

$$\tan\delta = \frac{E''}{E'} \tag{22}$$

When the material response is nonlinear a sinusoidal force input does not result in a sinusoidal output. Consequently a more general definition for damping is needed. In the literature, such cases are dealt with using the concept of energy dissipation [13]. Once the material constitutive information is well defined, it is easier to characterize the viscous energy dissipation over a cycle under harmonic input through the area under the hysteresis loop. This definition of the dissipated energy is valid regardless of the linearity or nonlinearity of the material behavior. With reference to the material model discussed above, the dissipated energy over a cycle can be written as:

$$W_d = \sum_{i=1}^{n=5} \int_t \int_v (\mathbf{T}^{Vi} : \overline{\mathbf{D}}^{Vvi}) dv dt \tag{23}$$

and the stored energy at any time τ is given by

$$W_s(\tau) = \int_0^\tau \int_v (\mathbf{T}^N : \overline{\mathbf{D}}) dv dt + \sum_{i=1}^{n=5} \int_0^\tau \int_v (\mathbf{T}^{Vi} : \overline{\mathbf{D}}^{Vei}) dv dt \tag{24}$$

and the average stored energy over a cycle with time period T is given by,

$$W_s^{avg} = \frac{1}{T} \int_0^T W_s(\tau) d\tau \tag{25}$$

There are five terms in the dissipated energy expression in Eq. (23) corresponds to the viscous dissipation related to the five dashpots in the model. Similarly in the stored energy expression, the 1st term corresponds to the energy stored due to the nonlinear spring, and the summation sign includes contribution from the linear springs. The nonlinear material can store a different magnitude of energy in tension (during the loading part of the sinusoid loading) than in compression cycle (the unloading part). In such cases, one needs to take the average stored energy from the tension and compression cycle as given in Eqn. 25. The specific damping capacity is then defined as given in [13],

$$\psi = \frac{W_d}{W_s^{avg}} \tag{26}$$

Further for linear viscous materials, the specific damping capacity can be related to $\tan\delta$ as,

$$\psi = 4\pi \tan\delta \tag{27}$$

therefore the ratio of $\frac{\psi}{4\pi}$ is termed the loss factor. Since the material damping measurements are performed in DMA tests, where the output is obtained in the linear viscoelastic regime in terms of $\tan\delta$, the computed loss factor in the present study will be presented as the damping measurements for the composites.

3. Results and discussion

As mentioned earlier, two dimensional plane strain simulations are performed by varying the different geometric features of the RVE in Fig. 1. The macroscopic normal strain ϵ_{xx} (see Fig. 1) is used to drive the deformation of the entire RVE in the axial direction, which satisfies the kinematic periodic boundary conditions and equilibrium. Since our particular interest lies in characterizing the damping behavior of the composites, a harmonic excitation is considered with a frequency of 1 Hz with a macroscopic strain amplitude of 0.1%. It is important to note that polymeric materials are highly strain rate/frequency dependent. Hence, by changing the external frequency or the strain amplitude one can achieve different mechanical responses for the above designed composites. In the present set of simulations, the metal sheets are considered to be of steel with an elastic modulus of 210 GPa with no damping. The thickness of the steel is 50 μm and kept fixed unless otherwise mentioned. The material constants for UMPU2 are listed in the Table 1.

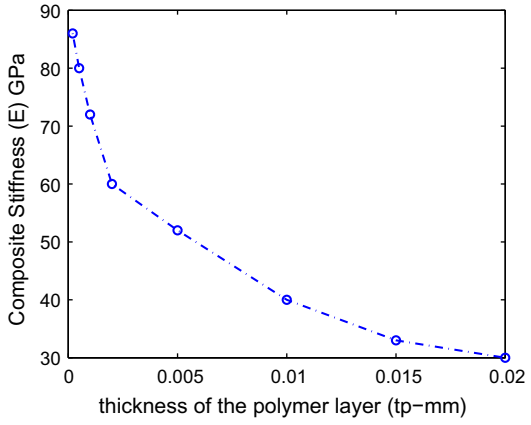

Fig. 9. Composite stiffness (axial) as a function of polymer layer thickness for $\delta = 0.1$ and $t_s = 0.05$ mm.

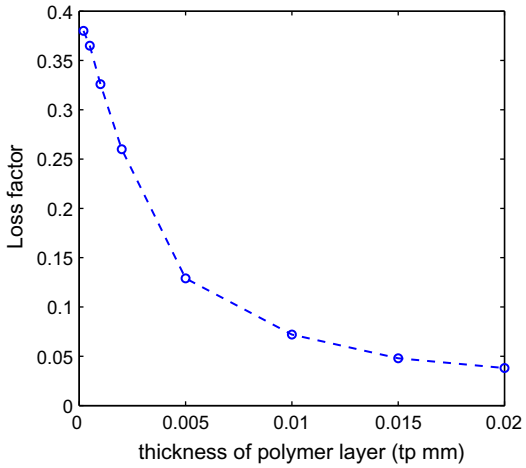

Fig. 10. Loss factor as a function of polymer layer thickness for $\delta = 0.1$ and $t_s = 0.05$ mm.

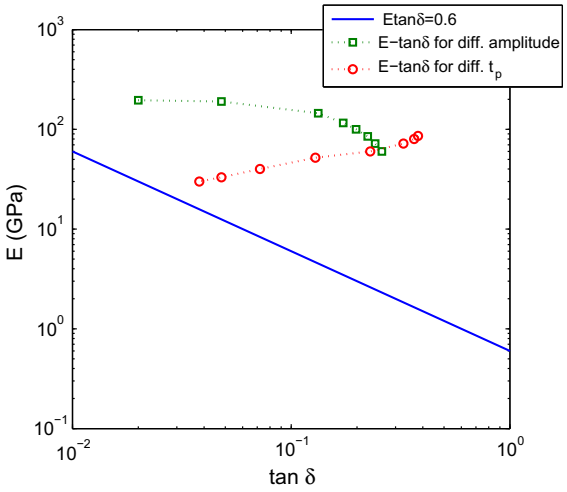

Fig. 11. Present simulation predictions in the stiffness-loss plot.

For the first set of simulations, the thickness of the polymer layer is chosen to be 2 μm and the amplitude of the waviness (a) is varied to study the effect of the wavy geometry on the mechanical response of the composite. A series of FE simulations is performed by varying the relative amplitude of the waviness (a/L) within the range 0.01–0.1. The calculated elastic modulus and the loss factor are presented as functions of the relative amplitude variation in Figs. 7 and 8, respectively. It is observed that – when the relative amplitude of the waviness is very small, i.e. 0.01, the limiting case is achieved with the elastic modulus of the composite being nearly the same 196 GPa as that of steel, and the damping is very low at $\frac{\psi}{2\pi} = 0.02$. However, as the amplitude of the waviness increases, the modulus decreases gradually at first and then more rapidly, reaching 60 GPa when $a = 0.1$. Simultaneously, the energy dissipation increases within the polymer layer, as the waviness increases, resulting in an increased loss factor output.

In the second set of simulations the thickness of the polymer layer is varied and the influence of its variation on the mechanical response of the composites is studied. For this set of simulations the relative amplitude of the waviness is taken as $a = 0.1$ and the thickness of the steel sheet is chosen as $t_s = 50$ μm. Figs. 9 and 10 show the variation of the composite elastic modulus and loss factor as functions of the polymer layer thickness (t_p) for a fixed value of $t_s = 50$ μm. Both plots show decreasing trends as t_p increases. For the elastic modulus, the decreasing trend is quite obvious due to the increase in the volume fraction of polymer in the RVE. The polymer is the much softer material and increasing its thickness for a fixed steel sheet thickness will result in a lower composite stiffness. The prediction of higher damping with lower polymer layer thickness can be explained through the shear deformation mechanism. The wavy geometry of the steel sheets introduces significant shear deformation in the thin layer of sandwiched polymer. By the definition of the shear strain, $\left(\gamma = \frac{\Delta u}{t_p}\right)$ (where Δu is the relative displacement between the top and bottom polymer surface in the x direction), the strain increases significantly as (t_p) decreases. Further, the dissipated energy in the polymer layer can be expressed as:

$$W_d^{poly} \sim \gamma^2 V \tag{28}$$

where V is volume of the polymer layer. As $\gamma \sim \frac{1}{t_p}$ and $V \sim t_p$, the dissipated energy is proportional to $\frac{1}{t_p}$. By analogy, the stored energy in the polymer layer is also proportional to $\frac{1}{t_p}$. Finally, the specific damping capacity becomes,

$$\psi = \frac{W_d}{W_s} = \frac{W_d^{poly}}{W_s^{poly} + W_d^{steel}} \sim \frac{1/t_p}{1/t_p + 1/t_s} = \frac{t_s}{t_p + t_s} \tag{29}$$

where constant t_s represents the constant steel thickness layer. Following Eq. (29), as the thickness of the polymer layer t_p reduces, ψ increases and eventually the loss factor also. The calculated modulus and loss factor values from the two sets of simulations are plotted in the stiffness-loss map proposed by Lakes et al. [14] as shown in Fig. 11. It is interesting to note in Fig. 11, that both sets of results lies well above the Wang–Lakes line [14]. Further work is underway to establish optimum layer thicknesses, and layer waviness patterns to maximize, both the stiffness and damping simultaneously and the results presented in this paper are used as baseline values for comparison purposes.

4. Conclusions

In this paper, a nonlinear time-dependent model for polymers is used to establish a wavy, multi-layered, two material composite to simultaneously increase both stiffness and damping. The influences of layer waviness amplitude and material layer thicknesses are studied to understand how stiffness and damping are affected by a change in these parameter values. Remarkably, the steel-layered polymer wavy composites exhibit stiffness and damping values that lie well above the Wang–Lakes line, which is a map that shows the values of stiffness and damping that can be achieved by using known materials and their composite combinations. The results presented can be used to further advance the goal of designing composite materials that can exhibit unusual combinations of mechanical properties.

Acknowledgement

The authors would like to gratefully acknowledge the financial support provided by **Defense Advanced Research and Project Agency DARPA** (USA) to carry out this work under Project Manager Dr. Aaron Lauzarus, and also gratefully acknowledge the contribution of Dr. Bongjun Yeom and Prof. Nicholas Kotov in manufacturing and preparing the PU samples, in Chemical Engineering Department at the University of Michigan, Ann Arbor.

References

[1] Finegan IC, Gibson RF. Recent research on enhancement of damping in polymer composites. Compos Struct 1999;44:89–98.
[2] Barrett DJ. Damped composite structures. Compos Struct 1991;18:283–94.
[3] Hwang SJ, Gibson RF. The use of strain energy-based finite element techniques in the analysis of various aspects of damping of composite materials and structures. J Compos Mater 1992;26:2585–605.
[4] Meaud J, Sain T, Hulbert G. Waas A. M. Analysis and optimal design of layered composites with high stiffness and high damping; Int. Jl. of Solids & Structures, 2013, in press, http://dx.doi.org/10.1016/j.ijsolstr.2013.01.014.
[5] Mantena PR, Gibson RF, Hwang SJ. Optimal constrained viscoelastic tape lengths for maximizing damping in laminated composites. AIAA J 1991;29:352–63.
[6] Suarez SA, Gibson RF, Sun CT, Chaturvedi SK. The influence of fiber length and fiber orientation on damping and stiffness of polymer composite materials. Experimen Mech 1986;26:175–84.
[7] Gibson RF, Chaturvedi SK, Sun CT. Complex moduli of aligned discontinuous fiber reinforced polymer composites. J Mater Sci 1982;17:3499–509.
[8] Chaturvedi SK, Tzheng GY. Micromechanical modeling of material damping in discontinuous fiber three-phase polymer composites. Compos Eng 1991;1:49–60.
[9] Friend RD, Kennedy JM, Edie DD. Evaluating the fiber matrix interphase in metal matrix composites using dynamic mechanical analysis. Damping of multiphase materials, vol. 1. Materials Park, OH: ASM International; 1992. p. 123–35.
[10] Pratt WF, Rotz CA, Jensen CJ. Improved damping and stiffness in composite structures using geometric fiber wave patterns. Proc ASME Noise Control Acoust Div 1996;2:37–43.
[11] Pratt WF, Allen MS. Testing and characterization of highly damped structural materials. In: 33rd International SAMPE technical conference, vol. 2. Seattle, WA; 2001.
[12] Pratt WF, Finite element analysis of wavy composites. In: ASME 2005 international design engineering technical conference. California, USA; 2005.
[13] Martz EO, Lakes RS, Park JB. Hysteresis behaviour and specific damping capacity of negative Poisson's ratio foams. Cell Polym 1996;15:349–64.
[14] Lakes RS, Lee T, Bersie A, Wang YC. Extreme damping in composite materials with negative stiffness inclusions. Nature 2001;410:565–7.
[15] Qi HJ, Boyce MC. Constitutive model for stretch-induced softening of the stress-stretch behavior of elastomeric materials. J Mech Phys Solids 2004;52:2187–205.
[16] Qi HJ, Boyce MC. Stress–strain behavior of thermoplastic polyurethane. Mech Mater 2005;31:817–39.
[17] Arruda EM, Boyce MC. A three-dimensional constitutive model for the large stretch behavior of rubber elastic materials. J Mech Phys Solids 1993;41:389–412.
[18] Sain, T, Meaud J, Kitcher B, Arruda EM, Waas A., Rate dependent finite strain constitutive modeling of polyurethane and polymer-clay nano-composites, manuscript in preparation for Journal of the Mechanics and Physics of Solids.
[19] Arruda EM, Boyce MC, Qunitus-Bosz H. Effect of initial anisotropy on the finite strain deformation behavior of glassy polymers. Int J Plast 1993;9:783–811.
[20] Kheng E, Iyer HR, Podsiadlo P, Kaushik AK, Kotov NA, Arruda EM, et al. Fracture toughness of exponential layer-by-layer polyurethane/poly(acrylic acid) nanocomposite films. Eng Fract Mech 2010;77:3227–45.